



# Determining the pore structure and radial variability of moso bamboo (*Phyllostachys edulis*)

Xi Yang<sup>1</sup> · Xiaona Pang<sup>1</sup> · Xinge Liu<sup>2</sup> · Shumin Yang<sup>2</sup> · Xianjun Li<sup>1</sup>

Received: 8 August 2021 / Accepted: 21 March 2022 / Published online: 28 December 2022  
© The Author(s), under exclusive licence to Springer-Verlag GmbH Germany, part of Springer Nature 2022

## Abstract

The native pore structure and characteristic are the basis for studying the permeability, pretreatment and further processing of bamboo. Herein, the porosity, surface area, pore volume and pore size distribution of moso bamboo and their radial variabilities were investigated by a combination of mercury intrusion porosimetry (MIP), nitrogen adsorption and scanning electron microscopic image analysis. Bamboo has a wide porosity range (48~70%) that exhibits a quadratic polynomial relation to the radial position, and parenchyma tissue shows higher surface porosity (around 71%) compared to vascular bundles (50.5~20.3%). The cell wall pores uncovered by MIP and N<sub>2</sub> adsorption display the meso- to macropores abundant characteristics and the mesopores account for 54.5~62.4%. Different radial samples demonstrate the similar pore size distributions but variable volumes and surface areas (85.3~88.2 m<sup>2</sup>/g). The outer part of bamboo has these values smaller than that of middle and inner samples, revealing a more compact structure. The present work gives an in-depth view on bamboo pore structure and radial heterogeneity, which could provide the basis for pretreatment and subsequent development of value-added bamboo products.

## Introduction

Bamboo, a super-rich plant resource in Asia and South America, has merits of fast growth (reaching full height within 3–6 months), short rotation (3–5 years), superior mechanical performance and sustained utilization after one afforestation (Liese 1998; Scurlock et al. 2000; Jiang 2007). Hence, bamboo like wood has always served

---

✉ Xianjun Li  
lxjmu@csuft.edu.cn

<sup>1</sup> College of Materials Science and Engineering, Central South University of Forestry and Technology, No. 498, Shaoshan South Road, Tianxin District, Changsha 410004, China

<sup>2</sup> Key Laboratory of Bamboo and Rattan Science and Technology of the State Forestry Administration, Department of Biomaterials, International Center for Bamboo and Rattan, Beijing 100102, China

as tools, furniture, buildings and fuels for supporting human activity (Scurlock et al. 2000). With the advancement of technology, depletion of fossil fuel and anthropogenic environmental degradation, tremendous attention has been paid to sustainable, eco-friendly development based on biomass materials (Jiang et al. 2018). Therefore, the significant potential for value-added, efficient and diversified development of bamboo resource has been recognized.

The unique structure of bamboo is the key determinant of physical and mechanical performance. Natural bamboo culm possesses rigid vascular bundles embedded in parenchyma cells with a certain variation rule (Fei et al. 2016). In vascular bundles, the fibrous sclerenchyma cells provide mechanical support (Dixon and Gibson 2014) while the hollow vessels and sieve tubes transport water and nutrients for the bamboo culm. Parenchyma cells make up around 50% of bamboo culm and render the outstanding flexural ductility of bamboo (Chen et al. 2020). There is obvious porous body with a capillary system in the bamboo tissue, including cell lumens and vessels along the growth direction, intercellular spaces and pits (Li et al. 2020; Lian et al. 2020a). For sustainable function applications, the water, modifier or functional substance is generally permeated through the porous structure. Therefore, it is of great significance to systematically study the characteristics of pore structure for understanding the penetration and realizing the functional utilization of bamboo.

Previous researchers have paid considerable attention to the heterogeneity of structure and mechanical properties of bamboo culm in growth direction and diameter direction (Low et al. 2006). For example, more densely distributed vascular bundles and stronger mechanical properties are observed at outer instead of inner section along the diametric direction (Ogunwusi and Onwualu 2013). Hence, the pore structure stemming from vascular bundles and parenchyma tissues suffers from the difference along the radial direction. Recently, the bamboo pore structure influenced by different treatments (Ye et al. 2020; Su et al. 2021) and the ultrastructure of bamboo pits and the connectivity (Lian et al. 2020a; Liu et al. 2021) have gained much attention. However, the native pore structure, especially regarding their radial variability, has not yet been fully characterized.

For analyzing the porous structure of a material, various techniques including mercury injection porosimetry (MIP) (Plötze and Niemz 2011; Peng et al. 2015), gas adsorption methods (Yin et al. 2015), microscopic image analysis (Rajagopal et al. 2019), X-ray computer tomography (Li et al. 2013), solute exclusion (Stone and Scallan 1968) and nuclear magnetic resonance (Yao and Liu 2012) can be employed. One should be aware that each technique has its own advantages and shortcomings in characterizing the porous structure. MIP takes advantage of its simple principle, good stability and rapid detection speed across a wide range of pore sizes; hence, it is one of the most commonly used methods for analyzing the pore structure of many porous materials, such as wood (Plötze and Niemz 2011; Moura et al. 2005) and coal (Yao and Liu 2012). Moreover, gas adsorption, especially nitrogen adsorption method, typically imparts the information related to nanopores, showing a very different narrow pore range (Kimura et al. 2016). As is well known, electron microscopy has been widely used to study the morphology and structure of a material. Digital image processing of cross-sectional or top-view micrographs could provide

additional quantitative information, such as porosity, pore size and size distribution (Ziel et al. 2008).

In this work, comprehensive pore information including porosity, pore volume and pore size distribution of moso bamboo was investigated by using MIP, nitrogen adsorption and electron microscopic image analysis. The pore features of inner, middle and outer parts of bamboo were given to characterize the radial heterogeneity, and the underlying relationship between bamboo porosity and its radial position was determined. The main purpose is to offer a new interpretation in terms of pore structure that bamboo green and bamboo fibers own permeability worse than wood, difficult to be uniformly filled by other substances. It is also expected to provide a useful insight into determination of bamboo potential improvements and functional utilization.

## Materials and methods

### Materials

Moso bamboo (*Phyllostachys edulis*, 3~4 years old) culms were obtained from bamboo forests of Hunan province. Prior to the removal of the epidermal and endodermal layers, bamboo blocks with an axial length of ~2 cm and a thickness of about 8 mm were cut from the internodes. As illustrated in Fig. 1, ten longitudinal cuts were uniformly made along the radial direction of the cross section of bamboo blocks to facilitate better understanding of the radial porosity of bamboo. Furthermore, three parts including outer, middle and inner were also uniformly cut along the radial direction of the block, followed by cutting along the tangential direction to make small strips for mercury intrusion and nitrogen adsorption measurement.

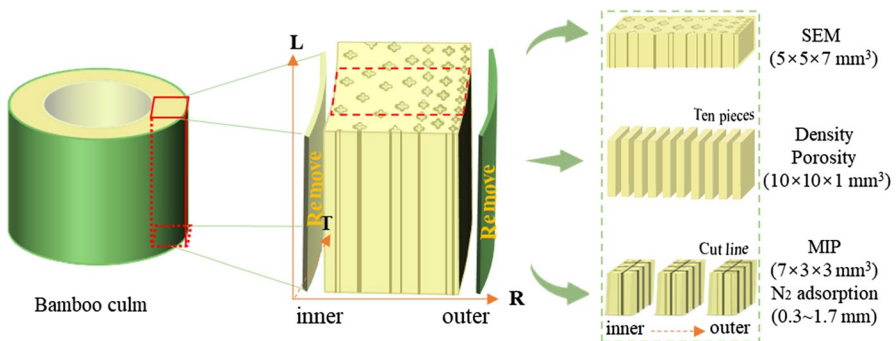


**Fig. 1** Schematic diagram for sample preparation (L, longitudinal direction; R, radial direction; T, tangential direction. Bamboo blocks were cut into ten pieces for overall porosity measurement and divided into three parts for MIP and nitrogen sorption measurement.)

## Porosity and density

For measuring the overall porosity of bamboo, ten radial pieces (1 ~ 10) and their seven duplicates from three different bamboo culms were employed. The calculation is based on the following equation:

$$P = (V_0 - V)/V_0 \times 100\% = (1 - \rho_0/\rho) \times 100\% \quad (1)$$

where  $P$  represents porosity of a material (%),  $V_0$  signifies the volume or apparent volume ( $\text{cm}^3$ ) in natural state,  $V$  is the absolute dense volume ( $\text{cm}^3$ ), and  $\rho_0$  and  $\rho$  are the volume density ( $\text{g}/\text{cm}^3$ ) and absolute density of a material, respectively. The absolute density for woody materials is around  $1.5 \text{ g}/\text{cm}^3$  (Du et al. 1992; Plötze and Niemz 2011). This measured porosity  $P$  includes all pores: open and closed.

## SEM image analysis

Moso bamboo blocks (without epidermal and endodermal layers) were cut into a cuboid shape with dimension of  $5 \times 5 \times 7$  (R)  $\text{mm}^3$ , and then, the transverse sections were polished by using a sliding microtome and air-dried for 12 h at room temperature. After sputter coating with nanogold, the surface morphology of bamboo blocks was observed by a scanning electron microscope (SEM, Zeiss Sigma 300) at an accelerating voltage of 5 kV. Later, the SEM images were imported into Image-Pro Plus software and the sizes were calibrated. Cell lumens could be accurately selected by automatic identification together with manual adjusting the boundary. The surface porosity can be acquired through dividing the total area of the selected lumens by the total area of the image. Besides, the diameters and the average values corresponding to the selected lumens can be obtained.

## MIP test

Mercury injection for capillary pressure measurement was carried out on a McPretic Autopore IV 9510 (United States) based on ISO standard 15901-1. Prior to the test, 2 ~ 3 g oven-dried (removing all bonded water and vapor at  $110^\circ\text{C}$  for 10 h) bamboo strips in the dimensions of 7(L)  $\text{mm} \times 3$ (T)  $\text{mm} \times (\sim 3)$ (R)  $\text{mm}$  was put into the sample chamber and sealed. The measurements were taken by incrementing the pressure approaching 300 MPa on a sample immersed in the non-wetting mercury. After the intrusion and extrusion, the total and incremental pore volume, pore surface area and porosity can be determined by the quantity (volume) of intruded mercury from low-pressure and high-pressure stations. Based on the hypothesis of bamboo composed of a porous body with various capillaries, the pore size distribution can be described by Washburn equation where pore size is inversely proportional to pressure (Li et al. 2018).

## Nitrogen adsorption measurement

The nitrogen adsorption and desorption of bamboo samples were measured on an Autosorb iQ apparatus at 77.3 K based on ISO standard 15901-2. Before that, 2 g 10–50 mesh power samples was first outgassed at 110°C for 10 h in a vacuum to eliminate the physically adsorbed gases (like water vapor) and impurities from the sample surfaces. Then the adsorption–desorption isotherms, Brunauer–Emmett–Teller (BET) surface area and pore size distribution were obtained.

## Results and discussion

### Radial porosity and image analysis

The overall porosity of ten equal bamboo pieces obtained along the radial direction is shown in Fig. 2a. From inner to outer parts of bamboo culm wall, the overall trend was increasing porosity followed by an obvious decline. According to the average values of porosity in Fig. 2a inset, the peak value of 70% appeared at the point one-third to one-half away from the innermost layer of the culm wall. The outermost layer had the lowest porosity (47%), and the porosity in the outer third of the culm wall was distinctly lower than that in other parts of the wall. This is because most fibers have barely visible lumens and fiber percentage is distinctly higher in the outer third of the bamboo culm wall (Li 2004). As a result, the bamboo porosity was strongly correlated with the radial position, and a quadratic polynomial fitting was made with correlation coefficient arriving at 0.95.

Figure 3 shows the microstructures of bamboo transverse section. Consistent with other observations, 50–80% of the vascular bundles were located in the outer third of the culm wall, 10–35% in the middle and only 10–20% in the inner part for moso bamboo (Fujii 1985) (Fig. 3a). The morphologies of vascular bundles and the lumen diameters of various cells were of significant difference

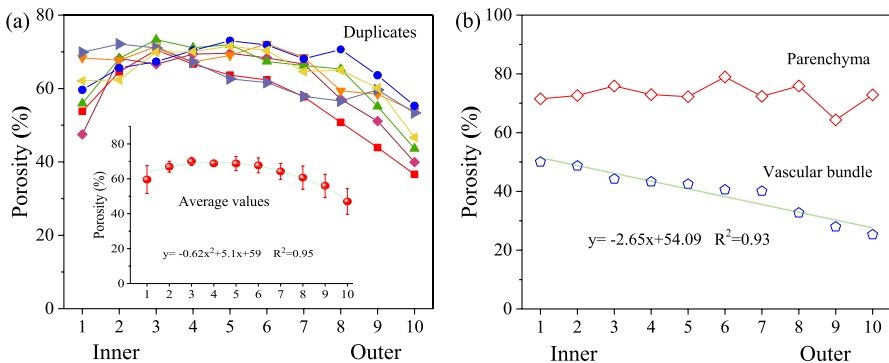


**Fig. 2** Overall porosity of ten radial bamboo pieces (a) and surface porosity of vascular bundles and parenchyma (b) based on SEM image analysis. The inset indicates the relation between average values of porosity and radial position

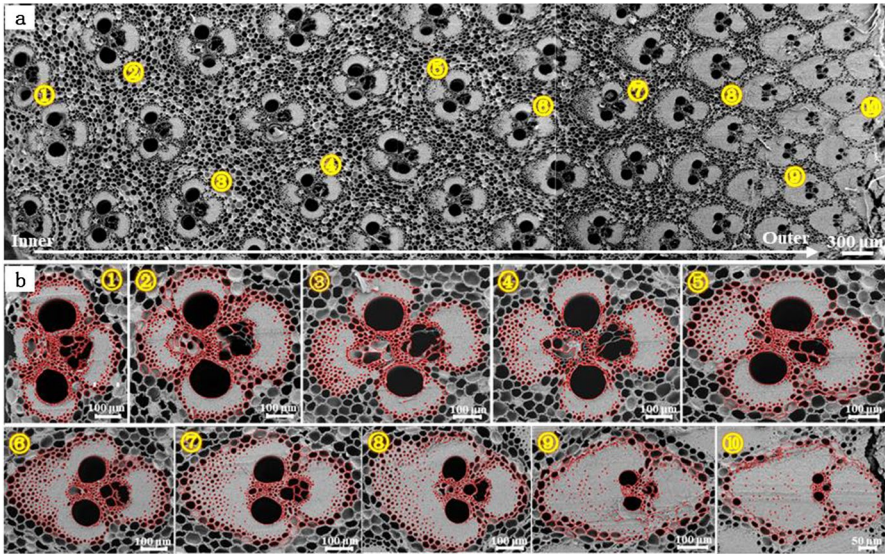


**Fig. 3** SEM images of moso bamboo at different radial positions (a) and image processing of ten vascular bundles based on Image-Pro Plus software (b)

along the radial direction. Further, ten images (Fig. 3b) of vascular bundles with higher magnification were obtained, as numerically marked in Fig. 3a. The porosity of vascular bundles and parenchyma tissue was subsequently calculated based on Image-Pro Plus software. As shown in Fig. 2b, the surface porosity of vascular bundles presented a near linear descent from 50.5 to 20.3% while the surface porosity of parenchyma tissue was maintained at around 71%, along the radial direction from the inner to the outer part of the culm wall. It means that the difference of bamboo radial porosity is mainly determined by vascular bundles instead of parenchyma tissue.

To distinguish which cells account for the radial variability in the porosity of bamboo or vascular bundles, the lumen diameters of fibers, parenchyma cells, metaxylem vessels, protoxylem vessels and sieve tubes were calculated, and the results are shown in Fig. 4. The average lumen diameters of fibers and parenchyma cells were basically unchanged along the radial direction up to the point one-fifth away from the bamboo outermost layer (Fig. 4a). Similarly, the average diameter of sieve tubes obviously also declined at one-fifth of the outermost layer. As for metaxylem vessels, its mean diameter decreased sharply at the outer part of bamboo (Fig. 4b). Differently, the mean lumen diameter of protoxylem vessels exhibited reduced values at both the innermost layer and outer third of the culm wall. It can be speculated that the radial variation in porosity was predominantly influenced by the difference of protoxylem vessels from radial inner to outer part of culm wall.

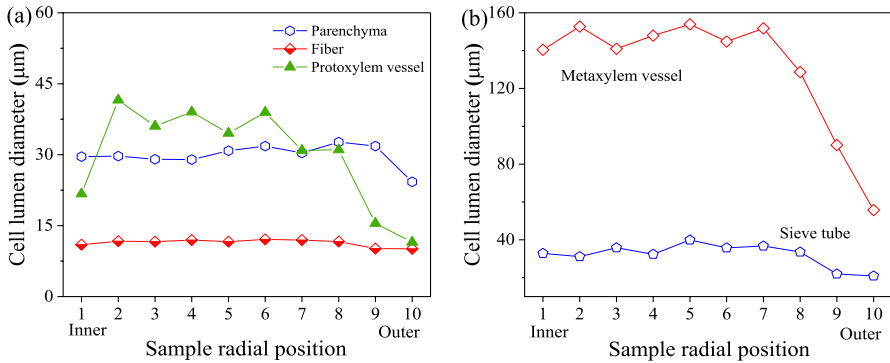


**Fig. 4** Lumen diameters of fibers, parenchyma, protoxylem vessels (a) and metaxylem vessels and sieve tubes (b) from radial inner to outer part of bamboo

## MIP analysis

Mercury intrusion porosimetry is an efficient and common method to determine porosity, pore size distribution and pore volume in porous materials (Plötze and Niemz 2011). Bamboo culm contains various lumens of fiber, vessel, sieve tube and parenchyma that can be regarded as a porous body with different capillary sizes, and the mercury can be pressed into the capillaries from large to small pores. The mercury intrusion–extrusion curves of three bamboo samples are shown in Fig. 5a–c. The incremental mercury intrusion curves are also given to demonstrate the detailed differences in mercury intrusion.

At the lower-pressure stage of 0–10 psia, the mercury gradually got into the macropores and the inner sample displayed apparently more macropores than middle and outer samples. With the further increment of pressure, the intake of mercury increased slowly because it is hard for mercury to get into smaller pores and the energy is primarily for compressing bamboo strips. It is noticeable that these pores were the most in the inner sample and the least in the outer sample. As the pressure surpasses 10,000 psia, the mercury was pressed into small capillaries and the intake had a vigorous growth. The cumulative intrusions of inner and middle samples were about one time larger than that of outer sample, suggesting the worse porosity of bamboo outer sample. Compared to the steep intrusion curves, the extrusion curves were more flat lines because the bamboo samples retained the overwhelming majority of mercury inside the pores. This phenomenon was attributed to the interconnectivity of the pores within bamboo, like wood (Ding et al. 2008).

The threshold pressure is adopted to determine when the mercury can easily enter the pores as well as to explain a connected pore network (Hu et al. 2017b). From Table 1, a lower threshold pressure (0.9 psia) of middle sample corresponded to a higher uptake of mercury (1.37 mL/g) and a higher level of porosity (70.9%), indicating the easier for mercury entering into the pores. The calculated porosity gradually augmented from the outer to the inner part of bamboo. Thus, the outer sample had a threshold pressure of 2.18 psia and the lowest porosity of 53%. Though outer sample

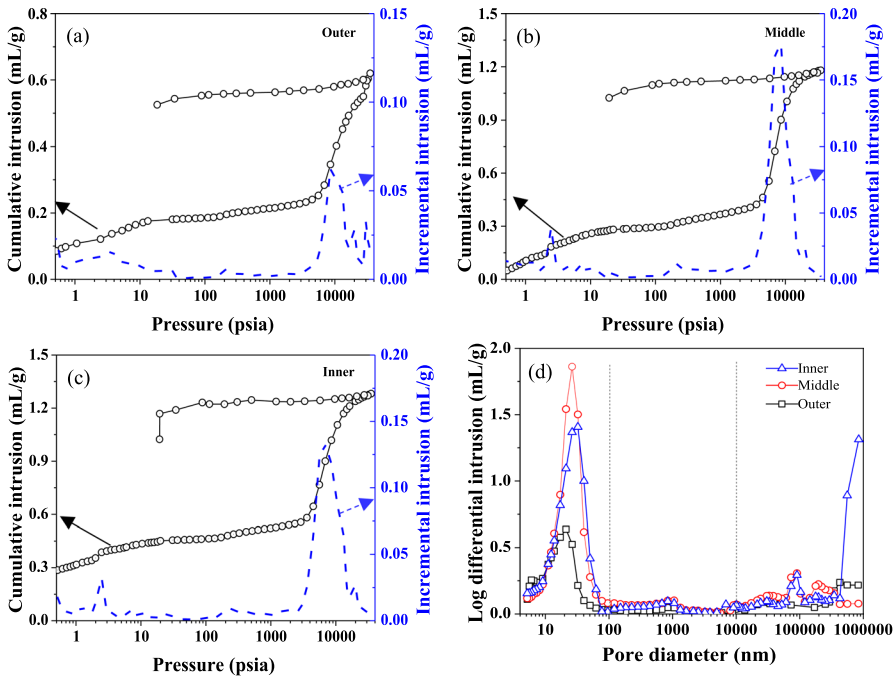


**Fig. 5** Mercury intrusion–extrusion curves of bamboo outer (a), middle (b) and inner (c) samples, and the corresponding differential pore size distribution (d)

**Table 1** Pore structural parameters based on mercury porosimetry

Samples	Relative pore volume/%				$P_t$ /psia	$V_T$ /mL/g	$r_{av}$ /nm	$S_T$ /m <sup>2</sup> /g	$\phi$ /%
	Pore size > 10 $\mu$ m	Pore size [10–0.1] $\mu$ m	Pore size [100–50] nm	Pore size [50–5] nm					
Outer	28.9	6.8	1.9	62.4	2.18	0.57	22.6	85.3	53.1
Middle	20.0	8.3	2.6	55.2	0.90	1.37	35.6	88.2	70.9
Inner	34.8	7.5	3.1	54.6	0.92	1.28	35.5	86.2	72.5

$P_t$  threshold pressure,  $V_T$  total volume of mercury,  $r_{av}$  average pore diameter,  $S_T$  total surface area,  $\phi$  porosity

displayed a smaller threshold pressure than larch wood (3.02 psia), larch wood had a higher porosity (70.18%) owing to its more abundant pores (Zhao et al. 2021). Moreover, the porosity determined with MIP was slightly lower than the overall porosity ( $P$ ) in Fig. 2a. It is reasonable because MIP porosity only accounted for the percentage of open pores that mercury accessed. In addition, according to the extended explanation of threshold pressure from Hu et al. (2017b), each change in threshold pressure is an indicator of mercury entering a different pore size. In the incremental mercury intrusion curves, each sample showed several changes (inflection point), demonstrating that



bamboo, whichever radial part, was endowed with a complex and similar hierarchical porous structure. The hysteresis between mercury intrusion and extrusion curves can also be applied to assess the degree of complexity in sample pores (Giesche 2006). A larger hysteresis (the ratio of mercury extrusion to intrusion) implies a higher degree of complexity.

To characterize the overall pore size distribution, pore sizes based on peak pore size and distribution range were calculated from the differential pore size distribution diagram (Fig. 5d). Clearly, three samples had similar curves and exhibited unimodal distributions, being different from most wood samples with bimodal distributions (Zhao et al. 2021). The apertures ranging between 5 and 100 nm were the majority, which might correspond to microvoids/plasmodesmata in pit membranes or cell wall capillaries. Liu et al. (2021) reported that pit membranes feature plasmodesma with a diameter of 40–100 nm, allowing direct flow of molecules between adjacent cells. The outer sample possessed the most available aperture at 21.1 nm, and the value increased to 26.3 and 32.4 nm for middle and inner samples. The corresponding mercury intake of middle sample was larger than that of inner and outer samples. The middle sample exhibited the most abundant macropores ranging from 100 to 1330 nm that might stem from the intrinsic pits and tiny voids. According to the previous literature (Liu et al. 2019), moso bamboo vessels had 0.9–2.7  $\mu\text{m}$  wide pit apertures and fibers exhibited smaller pit apertures, accompanied by narrow pit canals.

Though there is a small amount of pores distributed in 1.3–10  $\mu\text{m}$ , an increased quantity of pores with sizes bigger than 10  $\mu\text{m}$  was observed, especially in middle part of bamboo. These pores included various cell lumens as well as some smaller cell openings. According to the calculated diameters of cell lumens in Fig. 3, the pores around 33  $\mu\text{m}$  mostly originated from parenchyma lumens and the pores around 90  $\mu\text{m}$  were mainly from metaxylem vessels of bamboo. These measured pore sizes were slightly smaller than the corresponding real values, which is a consequence of the limitation of ink-bottle effect (Webb and Orr 1997). Usually, cell lumens would only get filled with mercury at the Kelvin–Laplace intrusion pressure of the pits and microvoids (Li et al. 2015; Vitas et al. 2019), leading to an overestimation of the volume of small pores (i.e., pits and microvoids) and an underestimation of the proportion of larger pores (i.e., cell lumens) (Chen 2012). From the log differential intrusion curves, three distinct pore groupings were clearly observed, namely, pore sizes of 1000–10, 10–0.1 and 100–5 nm. The relative pore volumes (%) are given in Table 1, which exhibited different proportions among three radial samples. Obviously, the mesopores (5–50 nm) accounted for more than one-half and no micropores (<2 nm) can be observed by MIP. The outer sample showed the higher proportion of mesopores than the other two samples, but its surface area (85.3  $\text{m}^2/\text{g}$ ) and pore volume (0.57  $\text{mL}/\text{g}$ ) were clearly smaller than the middle (88.2  $\text{m}^2/\text{g}$  and 1.37  $\text{mL}/\text{g}$ ) and the inner samples (86.2  $\text{m}^2/\text{g}$  and 1.28  $\text{mL}/\text{g}$ ).

### Nitrogen adsorption analysis

In Fig. 6a, the  $\text{N}_2$  adsorption–desorption isotherms of outer, middle and inner part of bamboo were almost irreversible and could be classified into type II and type IV

with H3 hysteresis loop, according to the international union of pure and applied chemistry (IUPAC) classification system (Thommes et al. 2015). At relatively low pressure ( $<0.1$ ), the quantity of adsorbed  $N_2$  of three samples was close to 0, indicating that the micropores of bamboo were rather poor. With incrementing pressure ( $0.1 < P/P_0 < 0.8$ ), the isotherm curves showed a linear and slow climb without a distinct inflection point, compared to type II isotherm, which implied the main existence of single-layer adsorption (Kuila and Prasad 2013). With further increase in pressure ( $0.8 < P/P_0 < 1.0$ ), the adsorption isotherms rose rapidly, which indicated the occurrence of multilayer adsorption and corresponded primarily to the filling of mesopores and macropores (Wang et al. 2019). When the relative pressure was close to 1, the adsorption isotherms were still climbing without a platform, suggesting that the adsorption was not saturated and there is a certain amount of macropores. The desorption branches were irreversible and showed steep decline at the relative pressure larger than 0.5. All desorption isotherms were almost coincident with the adsorption isotherms, meaning the small and similar hysteresis loop.

Type H3 hysteresis loop indicates the presence of layered slit pores with a relatively broad size distribution extending to the macropore domain. As shown in Fig. 6b, the pore size distributions of three radial samples were illustrated based on Barrett–Joyner–Halenda (BJH) method (Galarneau et al. 1999) and adsorption branches. Majority of the accessible pores exhibited diameters between 3 and 200 nm with several peaks in the pore size distribution curves. Specifically, the outer sample presented a larger peak at 3.3 nm than middle and inner samples, whereas the middle sample showed peak values at both 86 nm and 242 nm, and the inner part had a peak value at 5.6 nm. The BET specific surface areas of moso bamboo are 0.365–0.465  $m^2/g$ , smaller than that of Chinese fir (0.787–2.088  $m^2/g$ ) (Yin et al. 2015). The tiny surface areas obtained by  $N_2$  adsorption method are below the values from MIP method (Table 1), which is consistent with the report from Plötze and Niemz (2011). Except for the overestimated area from MIP micropores, the small area from  $N_2$  absorption might be related to the small quantity of nanopores, such as pits, microvoids and cell wall capillaries, due to the multilayer cell wall of both fiber and parenchyma (Hu et al. 2017a; Lian et al. 2020b; Liu et al. 2021). In addition,

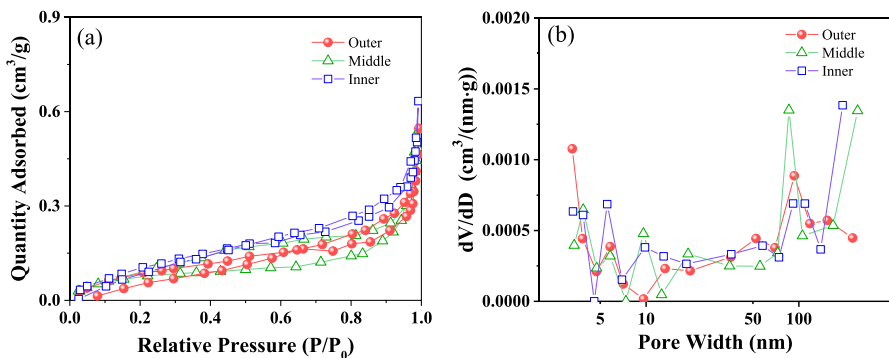


**Fig. 6**  $N_2$  adsorption–desorption isotherms (a) and pore size distributions (b)

the oven-dried bamboo samples may yield small specific surface area, according to the comparative mesoporous structure of air-dried and never-dried wood pulp by Kimura et al. (2016).

## Conclusion

In this study, pore information including porosity, volume, surface area, pore shape and pore size distribution of moso bamboo was systematically investigated by SEM image analysis, MIP and N<sub>2</sub> adsorption. The radial heterogeneity of the pore structure was also studied. It was indicated that bamboo porosity (48~70%) was in a quadratic polynomial relation to its radial position, and parenchyma tissue showed higher porosity (71%) compared to vascular bundles (50.5~20.3%). Bamboo samples exhibited a mixed sorption isotherm of type II and type IV and H3-type hysteresis loops, confirming the presence of slit-shaped meso- and macropores. According to the mercury intrusion curves and distributions of pore aperture, the mesopores accounted for 54.5~62.4% and the pore volumes were 0.57~1.37 mL/g. Different radial samples demonstrate similar pore size distributions but variable volumes and surface areas. In the outer part of bamboo, these values are smaller than in the middle and inner samples, revealing a more compact structure. The results could contribute to the explanation of poor impregnation of bamboo, especially at the outer part, and provide reference for subsequent processing or the development of value-added bamboo products.

**Acknowledgements** This work was financially supported by National Natural Science Foundation of China (No. 31901375; No. 32071852), Natural Science Foundation of Hunan Province (No. S2022JJQNJJ0900), the Foundation of Central South University of Forestry and Technology (2018YJ033) and the Science and Technology Innovation Program of Hunan Province (2020RC4049).

**Author contributions** All the authors have accepted responsibility for the entire content of this submitted manuscript and approved submission.

## Declarations

**Conflict of interest** On behalf of all authors, the corresponding author states that there is no conflict of interest.

## References

- Chen M, Ye L, Li H, Wang G, Chen Q, Fang C, Dai C, Fei BH (2020) Flexural strength and ductility of moso bamboo. *Constr Build Mater* 246:118418
- Chen Y (2012) Adsorption performance and characterization of porous materials. In: Preparation and characterization of porous materials (2 edn). University of science and technology of China Press, Hefei, pp 15–16.
- Ding WD, Koubaa A, Chaala A, Belem T, Krause C (2008) Relationship between wood porosity, wood density and methyl methacrylate impregnation rate. *Wood Mater Sci Eng* 3:62–70
- Dixon PG, Gibson LJ (2014) The structure and mechanics of Moso bamboo material. *J R Soc Interface* 11:20140321
- Du F, Zhang J, Lin W (1992) A study on bamboo density. *J Bamboo Res* 1(11):50–58

- Fei BH, Gao ZM, Wang J, Liu ZJ (2016) Biological, anatomical, and chemical characteristics of bamboo. Elsevier, Netherlands, pp 283–306
- Fujii T (1985) Cell-wall structure of the culm of Azumanezasa (*Pleioblastus chino* Max.). Mokuzaï Gakkaishi 31:865–872
- Galarneau A, Desplandier D, Dutartre R, Di Renzo F (1999) Micelle templated silicates as a test-bed for methods of pore size evaluation. Microporous Mesoporous Mater 27:297–308
- Giesche H (2006) Mercury porosimetry: a general (practical) overview. Part Part Syst Char 23:9–19
- Hu KL, Huang YH, Fei BH, Yao CL, Zhao C (2017a) Investigation of the multilayered structure and microfibril angle of different types of bamboo cell walls at the micro/nano level using a LC-PolScope imaging system. Cellulose 24:4611–4625
- Hu Q, Zhang Y, Meng X, Li Z, Li M (2017b) Characterization of micro-nano pore networks in shale oil reservoirs of Paleogene Shahejie Formation in Dongying Sag of Bohai Bay Basin, East China. Pet Explor Dev 44:720–730
- Jiang ZH (2007) Bamboo and rattan in the world. China Forestry Publishing House, Beijing, pp 3–10
- Jiang F, Li T, Li YJ, Zhang Y, Gong A, Dai JQ, Hitz E, Luo W, Hu LB (2018) Wood-based nanotechnologies toward sustainability. Adv Mater 30:1703453
- Kimura M, Qi ZD, Isogai A (2016) Analysis of mesopore structures in wood cell walls and pulp fibers by nitrogen adsorption method. Nord Pulp Pap Res J 31(2):198–204
- Kuila U, Prasad M (2013) Specific surface area and pore-size distribution in clays and shales. Geophys Prospect 61:341–362
- Li P, Wu Q, Tao Y (2013) Fractal dimension analysis of void size in wood-strand composites based on X-ray computer tomography images. Holzforschung 67(2):177–182
- Li HT, Su JW, Zhang QS, Deeks AJ, Hui D (2015) Mechanical performance of laminated bamboo column under axial compression. Compos B Eng 79:374–382
- Li LL, Wang XM, Yan Y, Ping LJ (2018) Pore analysis of thermally compressed Scots pine (*Pinus sylvestris* L.) by mercury intrusion porosimetry. Holzforschung 72(1):57–63.
- Li ZH, Chen CJ, Mi RY, Gan WT, Dai JQ, Jiao ML, Xie H, Yao YG, Xiao SL, Hu LB (2020) A strong, tough, and scalable structural material from fast-growing bamboo. Adv Mater 1906308.
- Li XB. (2004) Physical, chemical, and mechanical properties of bamboo and its utilization potential for fiberboard and manufacturing. Master thesis, Louisiana State University, United States.
- Lian CP, Liu R, Zhang SQ, Yuan J, Luo JJ, Yang F, Fei BH (2020b) Ultrastructure of parenchyma cell wall in bamboo (*Phyllostachys edulis*) culms. Cellulose 27:7321–7329
- Lian CP, Zhang H, Liu XM, Luo JJ, Yang F, Liu R, Fei, BH (2020a) Uncovering the ultrastructure of ramiform pits in the parenchyma cells of bamboo [*Phyllostachys edulis* (Carr.) J. Houz.]. Holzforschung 74(3):321–331.
- Liese W (1998) The anatomy of bamboo culms. International Network for Bamboo and Rattan, Beijing
- Liu M, Chen ML, Liu MM, Fei BH (2019) Characteristics of pits in moso bamboo (*Phyllostachys edulis*) revealed by resin casting. Scientia Silvae Sinicae 55(4):196–202
- Liu R, Zhang S, Sempke K, Lian C, Fei BH (2021) Precise microcasting revealing the connectivity of bamboo pore network. Ind Crops Prod 170:113787
- Low IM, Che ZY, Latella BA (2006) Mapping the structure, composition and mechanical properties of bamboo. J Mater Res 21:1969–1976
- Moura MJ, Ferreira PJ, Figueiredo MM (2005) Mercury intrusion porosimetry in pulp and paper technology. Powder Technol 160:61–66
- Ogunwusi AA, Onwualu AP (2013) Prospects of multi-functional utilisation of bamboo in Nigeria. Chem Mater Res 2(8):58–61
- Peng LM, Wang D, Fu F, Song BQ (2015) Analysis of wood pore characteristics with mercury intrusion porosimetry and X-ray micro-computed tomography. Wood Res-Slovakia 60(6):857–864
- Plötz M, Niemez P (2011) Porosity and pore size distribution of different wood types as determined by mercury intrusion porosimetry. Eur J Wood Prod 69:649–657
- Rajagopal H, Khairuddin ASM, Mokhtar N, Ahmad A, Yusof R (2019) Application of image quality assessment module to motion-blurred wood images for wood species identification system. Wood Sci Technol 53:967–981
- Scurlock JMO, Dayton DC, Hames B (2000) Bamboo: an overlooked biomass resource? Biomass Bioenergy 19(4):229–244
- Stone JE, Scallan AM (1968) Structural model for the cell wall of water-swollen wood pulp fibers based on their accessibility to macromolecules. Cellulose Chem Technol 2(1):343–358

- Su N, Fang CH, Yu ZX, Zhou H, Wang X, Tang T, Zhang SQ, Fei BH (2021) Effects of rosin treatment on hygroscopicity, dimensional stability, and pore structure of round bamboo culm. *Constr Build Mater* 287:123037
- Thommes M, Kaneko K, Neimark AV, James PO, Francisco RR, Jean R, Kenneth SWS (2015) Physisorption of gases, with special reference to the evaluation of surface area and pore size distribution (IUPAC technical report). *Pure Appl Chem* 87.
- Vitas S, Segmehl JS, Burgert I, Cabane E (2019) Porosity and pore size distribution of native and delignified beech wood determined by mercury intrusion porosimetry. *Materials* 12:416
- Wang QQ, Chang SS, Tan YJ, Hu JB (2019) Mesopore structure in *Camellia Oleifera* shell. *Protoplasma* 256:1145–1151
- Webb PA, Orr C (1997) Analytical methods in fine particle technology. Micromeritics Instrument Corporation, USA
- Yao YB, Liu DM (2012) Comparison of low-field NMR and mercury intrusion porosimetry in characterizing pore size distributions of coals. *Fuel* 95:152–158
- Ye C, Huang Y, Feng Q, Fei BH (2020) Effect of hygrothermal treatment on the porous structure and nanomechanics of moso bamboo. *Sci Rep* 10:6553
- Yin J, Song K, Lu Y, Zhao G, Yin Y (2015) Comparison of changes in micropores and mesopores in the wood cell walls of sapwood and heartwood. *Wood Sci Technol* 49:987–1001
- Zhao JY, Yang L, Cai YC (2021) Combining mercury intrusion porosimetry and fractal theory to determine the porous characteristics of wood. *Wood Sci Technol* 55:109–124
- Ziel R, Haus A, Tulke A (2008) Quantification of the pore size distribution (porosity profiles) in micro-filtration membranes by SEM, TEM and computer image analysis. *J Membrane Sci* 323:241–246

**Publisher's Note** Springer Nature remains neutral with regard to jurisdictional claims in published maps and institutional affiliations.

Springer Nature or its licensor (e.g. a society or other partner) holds exclusive rights to this article under a publishing agreement with the author(s) or other rightsholder(s); author self-archiving of the accepted manuscript version of this article is solely governed by the terms of such publishing agreement and applicable law.